

Prestack depth migration with the Gabor transform

Yongwang Ma and Gary F. Margrave

ABSTRACT

Wavefield extrapolation with phase shift is currently a migration tool of importance. In this paper, we present a new prestack seismic depth migration algorithm using the Gabor transform with application to the Marmousi acoustic velocity model. The imaging results show a very promising depth imaging algorithm, which should compete with the best depth imaging algorithms. The Gabor depth imaging algorithm approximates generalized phase shift plus interpolation (GPSPI) wavefield extrapolation, in which exact lateral velocities are used in a wavefield extrapolator. Previously, Gaussian windows have been used in the Gabor wavefield extrapolation algorithm. Each of these Gaussian windows is a ‘full-length’ window, with the same dimension as lateral velocity structures. Programs have been coded with the adaptive windowing algorithm, which will substantially reduce redundancy of calculations in wavefield extrapolation related to repeated Fourier transforms. High computation efficiency is expected using these more compactly supported windows.

INTRODUCTION

Migration with phase shift (Gazdag, 1978) (also called wavefield extrapolation with phase shift) was invented to improve accuracy and efficiency in depth imaging compared to other wave-equation migrations such as ones using the finite difference method (Clarebout and Doherty, 1972; Loewenthal et al., 1976). Seismic wavefield extrapolation with phase shift is unconditionally stable and extends simply to higher dimensions (e.g., 3D) (Gazdag and Sguazzero, 1984), compared to other numerical wave-equation-based migration methods. Wavefield extrapolation with phase shift shows its promising features in migrating seismic data, especially, in 3D due to its accuracy, speed and relative simplicity. One of the difficulties of wavefield extrapolation with Gazdag (1978) phase shift method is that it can only accommodate uniform lateral velocity, which is unrealistic for many practical applications. In the real world, velocity structures are mostly heterogeneous with strong lateral velocity fluctuations. To address lateral velocity variations in phase-shift wavefield extrapolations, phase shift plus interpolation (PSPI) was proposed by Gazdag and Sguazzero (1984). The PSPI method is implemented using a set of reference (laterally homogeneous) velocities to calculate extrapolated wavefields and the final extrapolated wavefields are obtained by interpolating with specific velocities corresponding to certain lateral positions. Kosloff and Kessler (1987) used a generalized phase-shift (GPS), with which phase-shift wavefield extrapolation can be extended to arbitrary velocities using an eigenvalue decomposition technique for wave propagation in arbitrary velocity structures. Stoffa et al. (1990) came up with an alternative wavefield extrapolation algorithm, split-step Fourier migration, dealing with lateral velocity variation while keeping the advantages of the phase-shift method, i.e., accuracy and efficiency. Other phase-shift wavefield extrapolation methods such as ‘phase-screen propagator’ (Wu and Huang, 1992; Roberts et al., 1997; Rousseau and de Hoop, 2001; Jin et al., 2002) also provide for accurate imaging with abrupt velocity variations in such geological settings as salt-dome environments. The generalized phase-shift (GPS) method and the split-step Fourier method compute thin-lens phase de-

lay (related to velocity variations) in the space-frequency domain and calculate phase-shift due to velocity perturbations in the frequency-wavenumber domain. Jin and Wu (1998) tested windowed phase-screen propagators and showed improved results in depth imaging compared to those from old phase-screen methods. Margrave and Ferguson (1999) used a nonstationary phase shift (NSPS) method and a generalized phase shift plus interpolation (GPSPI) to improve migration results, where wavefield extrapolations were done totally in the Fourier domain using exact velocity variations. Our wavefield extrapolation method follows Jin and Wu (1998) and approximates GPSPI with a Gabor extrapolator. We also have control over speed and accuracy of Gabor wavefield extrapolations with the help of the adaptive windowing algorithm by Grossman et al. (2002). In the following sections, we will demonstrate the adaptive Gabor wavefield extrapolation algorithm and some imaging results created by these algorithms.

GABOR WAVEFIELD EXTRAPOLATION THEORY

The continuous Gabor transforms

The continuous Gabor transform pair is written as (following Margrave and Lamoureux (2001))

$$V_g s(x'_T, k_T) = \int_{\mathbb{R}} s(x_T) g(x_T - x'_T) \exp(-ix_T k_T) dx_T \quad (1)$$

and

$$s(x_T) = \int_{\mathbb{R}^2} V_g s(x'_T, k_T) \gamma(x_T - x'_T) \exp(ix_T k_T) dk_T dx'_T, \quad (2)$$

where x_T denotes transverse coordinates (e.g., $x_T = x$ in 1D, $x_T = (x, y)$ in 2D), $s(x_T)$ is the input signal, $V_g s(x'_T, k_T)$ is the Gabor spectrum of $s(x_T)$, $g(x_T - x'_T)$ is an analysis windowing function with its centre at x'_T , $\gamma(x_T - x'_T)$ is a synthesis windowing function, and k_T is the coordinate in the wavenumber domain corresponding to x_T , \mathbb{R} denotes real domain for integrations. Equation (1) is in fact a Fourier transform of a windowed version of signal $s(x_T)$.

Equation (1) is used to calculate the Gabor spectrum of $s(x_T)$; in order to recover the original signal $s(x_T)$ from its Gabor spectrum $V_g s(x'_T, k_T)$, analysis and synthesis windows must satisfy

$$\int_{\mathbb{R}} g(x_T) \gamma(x_T) dx_T = 1 \quad (3)$$

(Margrave and Lamoureux, 2001), which is called a partition of unity (POU). The analysis windows could be any kind of mathematical functions. However, in our wavefield extrapolation applications, we choose functions with a localization property. In this way, we may represent our wavefield extrapolator depending on local velocities with a small error. Gaussian windows are good candidates, and we have chosen them for this paper. We also choose the synthesis window as unity (a boxcar across the lateral dimension), that is, we do no localization in the synthesis process.

The discrete Gabor transforms

The discrete versions of Gabor transforms and POU (see equations (1), (2) and (3)) are expressed as (after Margrave and Lamoureaux (2001))

$$\hat{s}_{l,m} = \sum_{n \in \mathbb{Z}} s_n g_{l,n} \exp(-2\pi i n m / N), \quad (4)$$

$$s_n = \sum_{l \in \mathbb{Z}} \sum_{m \in \mathbb{Z}} \hat{s}_{l,m} \gamma_{l,n} \exp(2\pi i n m / N), \quad (5)$$

and

$$\sum_{l \in \mathbb{Z}} g_l \gamma_l = 1, \quad (6)$$

where l is associated with centres of windows, m is the index corresponding to the Fourier domain coordinates k_T , n is the index of the transverse coordinates x_T , and N is the total number of discrete samples of s_n .

Wavefield extrapolation with the Gabor transforms

The generalized phase shift plus interpolation (GPSPI) is formulated as (Margrave and Ferguson, 1999; Margrave et al., 2004)

$$\psi_P(x_T, z + \Delta z, \omega) = \int_{\mathbb{R}} \hat{\psi}(k_T, z, \omega) \hat{W}(k_T, x_T, \Delta z) \exp(-ik_T x_T) dk_T, \quad (7)$$

where

$$\hat{W}(k_T, x_T, \Delta z) = \exp(ik_z(x_T) \Delta z), \quad (8)$$

$$k_z(x_T) = \begin{cases} \sqrt{\frac{\omega^2}{v^2(x_T)} - k_T^2}, & \frac{\omega^2}{v^2(x_T)} > k_T^2 \\ i\sqrt{k_T^2 - \frac{\omega^2}{v^2(x_T)}}, & \frac{\omega^2}{v^2(x_T)} < k_T^2, \end{cases} \quad (9)$$

Δz is the step size of extrapolation in z (vertical) direction, ω is temporal frequency and $v(x_T)$ denotes lateral velocities along a slab with thickness Δz . Equation (7) extrapolates wavefields at depth z down to depth $z + \Delta z$ in the frequency-wavenumber domain.

The NSPS extrapolation is given as

$$\hat{\psi}_N(k_T, z + \Delta z, \omega) = \int_{\mathbb{R}} \psi(x_T, z, \omega) \hat{W}(k_T, x_T, \Delta z) \exp(ik_T x_T) dx_T. \quad (10)$$

To develop a Gabor approximation to equations (7) and (10), we introduce the approximation

$$\hat{W}(k_T, x_T, \Delta z) \approx \sum_{j \in \mathbb{Z}} \Omega_j(x_T) S_j(x_T) \hat{W}(k_T, \Delta z) \quad (11)$$

where Ω_j is a family of windows forming a POU (refer to equations (3) and (6)), $S_j(x_T)$ is a split-step Fourier operator for phase correction in the Gabor imaging, $\hat{W}(k_T, \Delta z)$ is a wavefield extrapolator with reference velocities v_j , which are

$$S_j(x_T) = \exp\left(i\omega \Delta z \left(\frac{1}{v(x_T)} - \frac{1}{v_j}\right)\right), \quad (12)$$

$$\hat{W}(k_T, \Delta z) = \exp(ik_z \Delta z) \quad (13)$$

and

$$v_j = \frac{\int_{\mathbb{R}} \Omega_j(x_T) v(x_T) dx_T}{\int_{\mathbb{R}} \Omega_j(x_T) dx_T}, \quad (14)$$

respectively. Notice that in equation (13), k_z is calculated with a formula similar to equation (9), using not the exact velocity $v(x_T)$ but the reference velocity v_j corresponding to a specific window Ω_j (see equation (14)).

Using approximate wavefield extrapolator (11) in (7) and (10) gives

$$\psi_P(x_T, z + \Delta z) = \sum_{j \in \mathbb{Z}} \Omega_j(x_T) S_j(x_T) \int_{\mathbb{R}} \hat{\psi}(k_T, z, \omega) \hat{W}(k_T, \Delta z) \exp(-ik_T x_T) dk_T \quad (15)$$

and

$$\hat{\psi}_N(k_T, z + \Delta z, \omega) = \sum_{j \in \mathbb{Z}} \hat{W}_j(k_T, \Delta z) \int_{\mathbb{R}} \Omega_j(x_T) S_j(x_T) \psi(x_T, z, \omega) \exp(ik_T x_T) dx_T. \quad (16)$$

A combination of approximate GPSPI and NSPS within a single extrapolation step Δz can be written as

$$\begin{aligned} \psi_{PN}(x_T, z + \Delta z, \omega) = & \sum_{j \in \mathbb{Z}} \Omega_j(x_T) S_j(x_T) \int_{\mathbb{R}} \left[\hat{W}_j(k_T, \frac{\Delta z}{2}) \sum_{m \in \mathbb{Z}} \hat{W}_m(k_T, \frac{\Delta z}{2}) \int_{\mathbb{R}} \Omega'_m(x_T) \right. \\ & \left. \cdot S_m(x_T) \psi(x_T, z, \omega) \exp(i k_T x_T) dx_T \right] \exp(-i k_T x_T) dk_T. \end{aligned} \quad (17)$$

Whether this combination scheme is more efficient and accurate than Gabor approximations with single GPSPI or NSPS method remains as an open research problem.

Gabor wavefield extrapolation with adaptive windowing method

If analysis windows in Gabor wavefield extrapolations are uniformly distributed along the lateral dimensions, we will, in most circumstances, have excessive redundancy in computations. That is, the algorithm without adaptive windowing basically calculates more windowed Fourier transforms than it requires. For example, we know that for homogeneous media, we only need one window (Ω) instead of many, where the GPSPI method degenerates into Gazdag (1978) Fourier migration (phase shift with constant velocity) in laterally homogeneous media. If the lateral velocity structures in a slab are not extremely inhomogeneous, we can use fewer windowed Fourier transforms in wavefield extrapolations than we do in rapidly varying velocity models. Adaptive windowing algorithms are suggested to deal with different types of lateral velocity structures met in Gabor wavefield extrapolations. At this time, we use the Grossman et al. (2002) algorithm, which makes use of lateral velocity gradients to determine the number of windows needed in wavefield extrapolations to satisfy certain imaging accuracy criteria. However, this algorithm does not consider phase errors in wavefield extrapolations. Thus in future work on Gabor wavefield extrapolations, we hope to supersede this windowing algorithm, though it works quite well to get spatially accurate images. A new windowing algorithm has been developed, which considers not only lateral velocity variation but also phase errors of the Gabor wavefield extrapolator (Ma and Margrave, 2005). With adaptive windowing algorithms, we can obtain a greatly improved computation efficiency in Gabor wavefield extrapolations. Without the adaptive windowing algorithm (with Gaussian windows), the Gabor imaging method spends as about 90 times amount of time as it requires with the adaptive windowing algorithm to image a typical velocity model (examples not shown here).

GABOR WAVEFIELD EXTRAPOLATION EXAMPLES

Impulse responses

An impulse response test is set up for examining the accuracy of the Gabor extrapolator. In the first example, we show an impulse propagating in a homogeneous medium (see Figure 1 (a) and (c)). The second example shown in Figure 1 (d) gives the results with the Gabor extrapolator in a laterally inhomogeneous medium. In Figure 1 (b), the grey area on the left side was a constant velocity of 2000 m/s, and the black region on the right side has a velocity of 4000m/s.

In both impulse response examples, the impulse sources were extrapolated in space to a depth of 200 meters with a step size of 10 meters. The sources were deployed at time about 0.34 second in traces (see Figure 1 (a)), the impulse sources back propagate to time about 0.24 second after they have been extrapolated 200 meters at a speed of 2000 m/s (see Figure 1 (c)). This shows that the Gabor extrapolator has done extrapolation correctly and accurately. The second example is used to show how wavefields are extrapolated in a medium with laterally abrupt velocity variation (see Figure 1 (b)). The extrapolation depth is also 200 meters. We can predict that in the left side (velocity 2000 m/s) the extrapolated impulses will be at 0.24 second; and that in the right side (velocity 4000 m/s) the extrapolated impulses will be at about 0.29 second (see Figure 1 (a)). We can see from Figure 1 (d) that the Gabor extrapolator gives correct extrapolation of those impulses in both the homogeneous and the step velocity models.

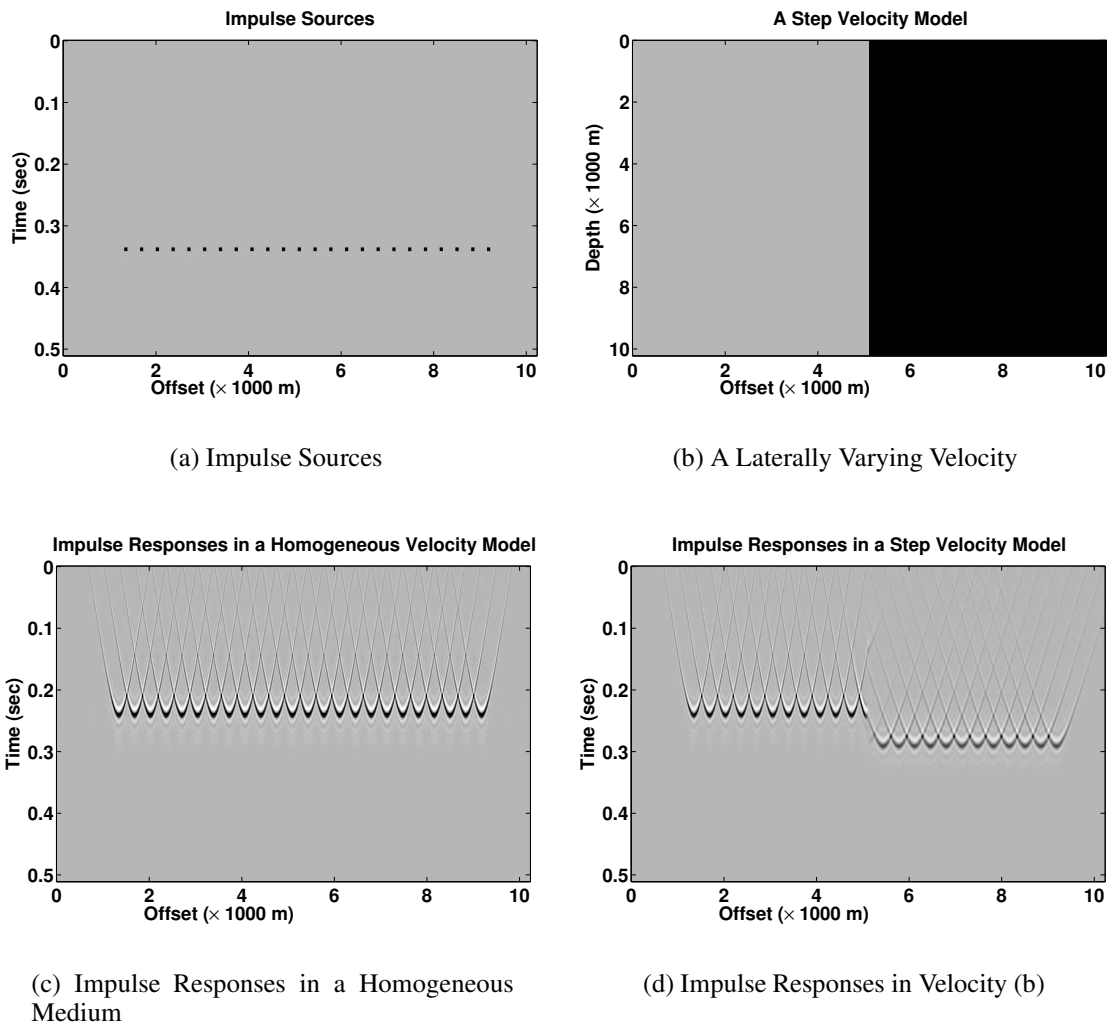


FIG. 1. Impulse Responses Calculated with the Gabor Extrapolator

Imaging Marmousi acoustic velocity structures

Marmousi synthetic data set has been widely used as a benchmark for testing depth imaging algorithms. The Marmousi velocity profile used in our depth imaging is shown in Figure 2 (a). In the Marmousi synthetic data set, we have 240 shot records, each of which has 96 traces, with time extending to about 2.9 seconds. For each shot record, there are 241 extrapolation steps with step size $\Delta z = 12.5$ meters.

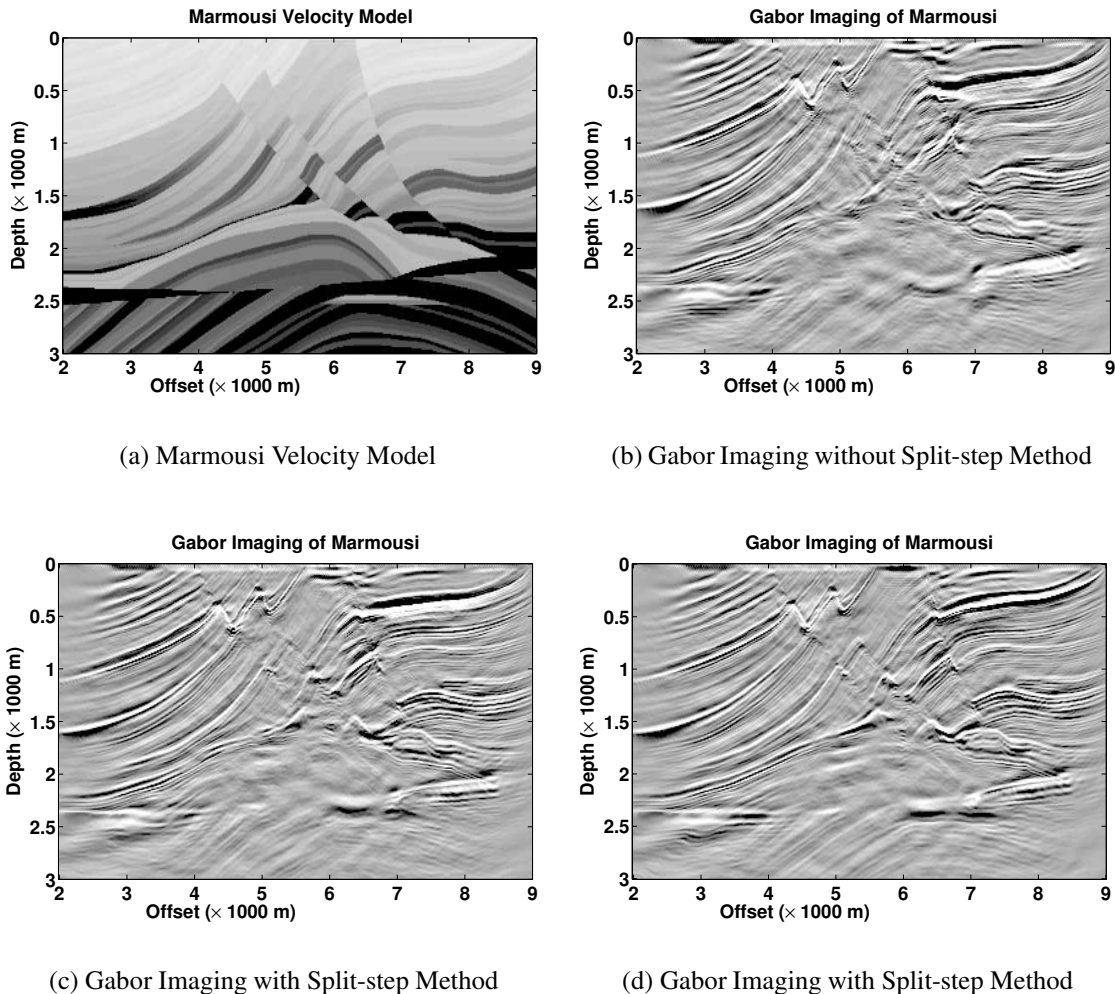


FIG. 2. Marmousi Velocity Model and Gabor Imaging Results. (a) windowing parameter factor=5 without the split-step Fourier operator to correct phases in wavefield extrapolation with the Gabor wavefield extrapolator; (b) windowing parameter factor=5 with the split-step Fourier operator to correct phases in the Gabor wavefield extrapolation; (c) windowing parameter factor=10 with the split-step Fourier phase corrections. We can see from these three imaging results that with more windows used, the imaging results are better (compare (b) and (c)), and that with the phase correction, the imaging results are also better (compare (c) and (d)). On the PC with a CPU of 3.0 GHz, for the Gabor imaging of Marmousi velocity model with factor=5, the CPU time is about 38 hours; if factor=10 is used, CPU time will nearly double.

Before we analyze the imaging results, we explain the parameter used in the adaptive windowing algorithm. We call this parameter ‘factor’, which is used to set the threshold

in terms of the relative velocity variation (related to the lateral velocity gradients). For example, when we stand in a window and let factor = 5, we mean that $1/5 = 20\%$ of the average velocity in the current window is set as the threshold; if velocity difference between the mean velocity of the current window and that of the next neighbouring window along the lateral dimension exceeds this threshold, we will not merge the next window into the current one. Otherwise, we do. That is, if the difference between the mean velocities of the current window and the next one is smaller than the threshold set by 'factor', the next window is merged with the current window and the new combined window works as the 'current' window. If not, we will leave the current window as it is and acquire the next as the 'current' window, and repeat the process until we reach the edge of the lateral dimension. For mathematical details of the algorithm, see Grossman et al. (2002). If 'factor' is smaller, fewer windows will be used, and vice versa.

In imaging results Figure 2 (b) and (c), we used a factor of 5. These are the cases in the Marmousi imaging with the most modest number of windows assigned by the adaptive windowing algorithm. We see that both are no better than the image in Figure 2 (d), where a factor of 10 is used. Looking at the fault regions and the bottom part of the images in Figure 2 and examining the target reservoir, from 6000 m to 7500 m at about depth 2500 m; we can see that the reservoir is adequately imaged in (d), but not in (b) and (c). We conclude that more windows means better imaging results. So with this parameter (factor) we can control the quality (accuracy) of the Gabor imaging. i.e, we can trade between accuracy and efficiency in the Gabor depth imaging.

Figure 2 (b) and (c) are used to show how the split-step Fourier correction plays an important role in the Gabor depth imaging. Figure 2 (b) shows the Gabor imaging result without the split-step Fourier correction; Figure 2 (c) shows the same result with the split-step Fourier correction. Both imaging results are calculated with the same windowing parameter, factor=5, which means there is no imaging difference caused by the adaptive windowing. Without the split-step Fourier operator to correct phase in Gabor extrapolations, the imaging result is very poor compared to the one with the split-step operator. Examining Figure 2 (b) and (c) in the lower parts of the images, we can nearly see the imaged reservoir in (c) but not in (b).

To see how the adaptive windowing algorithm works in the Marmousi velocity model, in Figure 3 we show 'windows versus the depth and the lateral coordinates (offsets)' corresponding to the dimensions of the Marmousi velocity model used in the Gabor imaging. The figure is created with the Gabor imaging process with a factor of 20 (a finer windowing scheme); the corresponding Gabor depth imaging result is shown in Figure 4 (a), to be compared to the image generated by the FOCITM.

To show how well the Gabor extrapolator works, we use a FOCITM (Margrave et al., 2004) Marmousi imaging result to compare with the Gabor Marmousi imaging result (see Figure 4 (a) and (b)). We see that, overall, the Gabor imaging algorithm gives a very good imaging result for the Marmousi velocity structures. Compared with the FOCITM imaging result, the Gabor imaging method yields a very clear image of the Marmousi velocity model, though the FOCITM seems to give more detailed and enhanced structural information in those over-thrust regions. The Gabor extrapolator may do as well as the

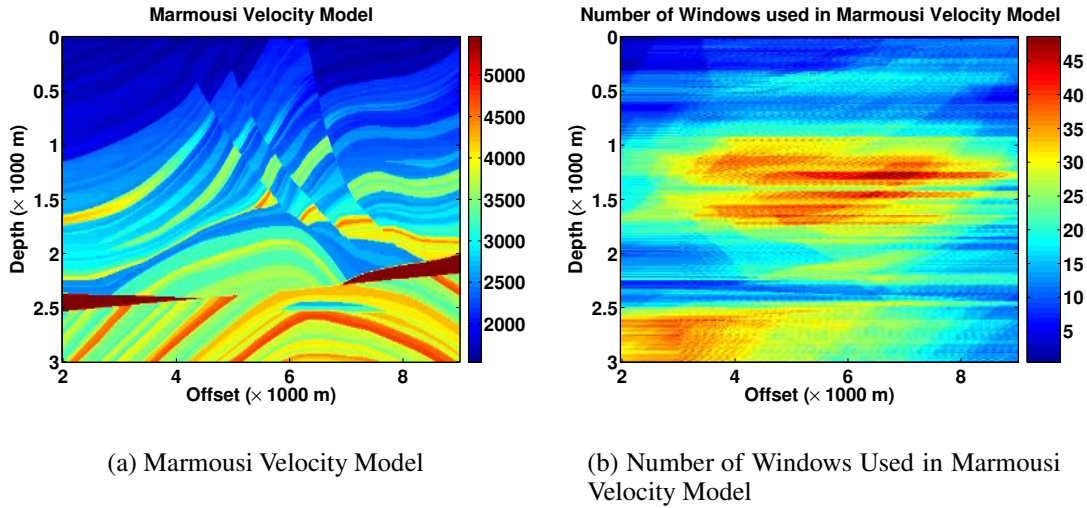


FIG. 3. Windowing Marmousi Velocity Model with the Adaptive Windowing Algorithm. In (a), the units of the scale on the right are in m/s; in (b), the units of the scale on the right are in number of windows. Note that the transverse coordinates in (b) is not the true coordinates. The figure in (b) consists of 240 columns of 'windows versus depth'. These columns are created during the shot migrations. Each of these 240 columns 'windows versus depth' corresponding to a velocity 'piece' adapted from the whole Marmousi velocity model used for a single shot migration. We put the true transverse coordinates into the figure to make it roughly comparable with the transverse coordinates in the velocity model (a) to see how the windows are distributed.

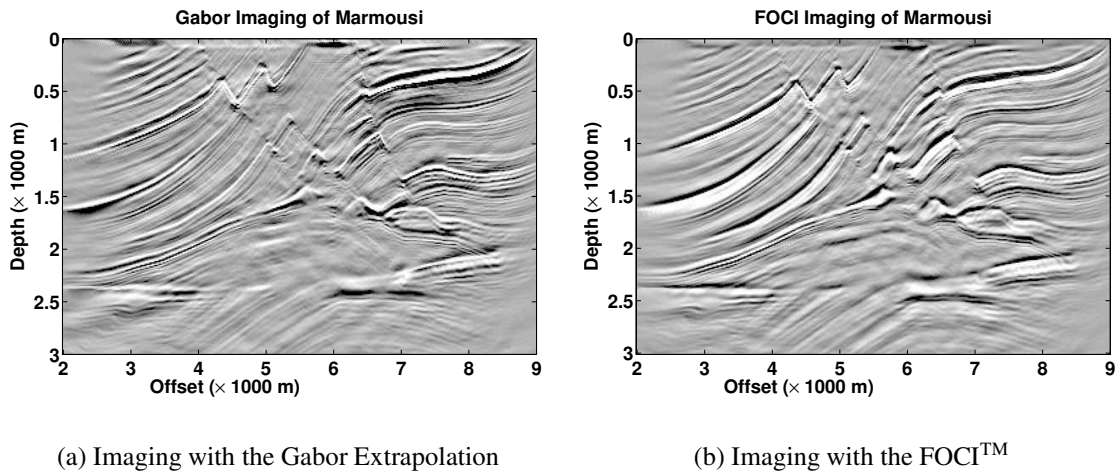


FIG. 4. Marmousi Imaging Results. (a) The Gabor imaging result with factor=20 in (a) was created by a PC (3 GHz CPU) in about 112 hours; (b) FOCI™ imaging result runs on a common PC for about 20 hours.

FOCITM in these regions with a more detailed windowing scheme. i.e., we can use more windows to get images that are comparable with the FOCITM in those over-thrust regions, but the processing time will increase.

In the lower part of Marmousi model, especially, the region of the anticline enclosing the target reservoir, both imaging methods do a good job. The Gabor method creates clearer image just above the anticline than the FOCITM does, while the FOCITM images better inside the anticline.

The Gabor extrapolator is slower than the FOCITM for comparable results. Nevertheless, we have hope to improve the accuracy and speed of imaging with the Gabor extrapolator by using some new adaptive windowing algorithms and different window sets.

CONCLUSIONS

The Gabor extrapolator is a very promising imaging tool in seismic depth migration. The Gabor imaging results have shown that we can get accurate depth images for complicated velocity structures such as the Marmousi acoustic velocity model, which is a solid basis for further research and exploration of the new imaging algorithm. The Gabor extrapolator can be used to image velocity structures as accurately as we may require. Computation (imaging) speed has been highly improved when the adaptive windowing algorithm is integrated into the Gabor wavefield extrapolation.

REFERENCES

- Clarebout, J. F., and Doherty, S. M., 1972, Downward continuation of moveout-corrected seismograms: *Geophysics*, **37**, 741–768.
- Gazdag, J., 1978, Wave equation migration with the phase-shift method: *Geophysics*, **43**, No. 7, 1342–1351.
- Gazdag, J., and Sguazzero, P., 1984, Migration of seismic data by phase shift plus interpolation: *Geophysics*, **49**, No. 2, 124–131.
- Grossman, J. P., Margrave, G. F., and Lamoureux, M. P., 2002, Fast wavefield extrapolation by phase-shift in the nonuniform Gabor domain: CREWES Research Report, **14**.
- Jin, S., and Wu, R., 1998, Depth migration using the windowed generalized screen propagators: *SEG Expanded Abstracts*, **17**, 1843.
- Jin, S., Xu, S., and Mosher, C. C., 2002, Migration with a local phase screen propagator: *SEG Expanded Abstracts*, **21**, 1164.
- Kosloff, D., and Kessler, D., 1987, Accurate depth migration by a generalized phase-shift method: *Geophysics*, **52**, No. 8, 1074–1084.
- Loewenthal, D., Lu, L., Roberson, R., and Sherwood, J. W. C., 1976, The wave equation applied to migration: *Geophys. Prosp.*, **24**, 380–399.
- Ma, Y., and Margrave, G. F., 2005, A new adaptive windowing algorithm for the gabor depth imaging: CREWES Research Report, **17**.
- Margrave, G. F., Al-Saleh, S. M., Geiger, H. D., and Lamoureux, M. P., 2004, The FOCITM algorithm for seismic depth migration: CREWES Research Report, **16**.
- Margrave, G. F., and Ferguson, R. J., 1999, Wavefield extrapolation by nonstationary phase shift: *Geophysics*, **64**, No. 4, 1067–1078.
- Margrave, G. F., and Lamoureux, M. P., 2001, Gabor deconvolution: CREWES Research Report, **13**.
- Roberts, P., Huang, L., Burch, C., Fehler, M., and Hildebrand, S., 1997, Prestack depth migration for complex 2d structure using phase-screen propagators: *SEG Expanded Abstracts*, **16**, 1282.
- Rousseau, J., and de Hoop, M. V., 2001, Modeling and imaging with the scalar generalized-screen algorithms in isotropic media: *Geophysics*, **66**, 1551.
- Stoffa, P. L., Fokkema, J. T., de Luna Freire, R. M., and Kessinger, W. P., 1990, Split-step fourier migration: *Geophysics*, **55**, 410–421.
- Wu, R., and Huang, L., 1992, Scattered calculation in heterogeneous media using a phase-screen propagator:

SEG Expanded Abstracts, **11**, 1289.